Analyst

RSC Publishing

PAPER

View Article Online
View Journal | View Issue

Cite this: *Analyst*, 2013, **138**, 7101

Enhanced peroxydisulfate electrochemiluminescence for dopamine biosensing based on Au nanoparticle decorated reduced graphene oxide†

Yuting Yan,[a] Qian Liu,[b] Kun Wang,*[a] Ling Jiang,[a] Xingwang Yang,[a] Jing Qian,[a] Xiaoya Dong[a] and Baijing Qiu[a]

Received 14th August 2013
Accepted 18th September 2013

DOI: 10.1039/c3an01533e

www.rsc.org/analyst

This work reports a novel strategy to amplify the electrochemiluminescence (ECL) signal of peroxydisulfate solution based on the Au nanoparticle decorated reduced graphene oxide (Au NP–RGO), and further an ECL biosensor for sensitive and selective detection of dopamine (DA) was constructed. Due to the synergistic amplification of Au NPs and RGO, the ECL signal of peroxydisulfate solution on the Au NP–RGO modified electrode was about 5-fold enhanced compared to that of the bare electrode with the ECL onset potential positively shifted from −1.2 V to −0.9 V. More interestingly, the ECL intensity of peroxydisulfate solution increased with the increase of DA concentration, based on which an ECL biosensor for DA determination was fabricated. The as-prepared solid-state ECL DA sensor showed a wide linear response of 0.02–40 μM with a detection limit of 6.7 nM ($S/N = 3$). Moreover, we expect this work would open up a new field in the application of peroxydisulfate solution ECL for highly sensitive bioassays.

Introduction

As a valuable detection method, electrochemiluminescence (ECL) has attracted great interest in analytical chemistry owing to its distinct advantages of simplicity, rapidity, sensitivity, controllability and low background.[1,2] In the past two decades, a number of ECL systems have been discovered and studied, including Ru complexes,[3,4] luminal,[5] quantum dots[6,7] and peroxydisulfate systems.[8] Among these different ECL reactions that have been classified, the kind of ECL system based on peroxydisulfate plays an important role and has been used in the fields of biosensors, aptasensors, and immunoassay.[8–14] However, the ECL emission generated from peroxydisulfate in aqueous solution was very weak, which was not adequate for sensitive analytical application.[10] Thus, great efforts have been focused on exploring effective methods to enhance the ECL of peroxydisulfate solution. For example, Yang *et al.* found that the ECL intensity of peroxydisulfate can be effectively enhanced on the C_{60}/didodecyldimethyl ammonium bromide films,[15] which showed potential applications in the field of ECL analysis. Using L-cysteine and Au nanoparticles (Au NPs) for amplifying the ECL signal of peroxydisulfate solution, Yuan's group further constructed a novel strategy for developing an immunosensor for cancer biomarker detection.[11] These results indicate that the ECL intensity of peroxydisulfate solution could be amplified effectively by incorporating nanomaterials, and to date, it is just the beginning of this fantastic topic.

Graphene and graphene-based nanocomposites, due to their abundant physical and chemical properties, have been widely explored for applications in many different fields from biosensors to diagnosing diseases.[16] Recently, more and more attention has been focused on graphene-based materials in ECL applications, by virtue of their effective amplification of the ECL signal in the fabrication of ECL biosensors.[17–19] For example, in our previous work, we found that the ECL intensity of CdS nanocrystals can be effectively enhanced by graphene, and a solid-state ECL H_2O_2 sensor was constructed successfully based on the graphene–CdS nanocomposites.[20] Due to the synergistic amplification of 3,4,9,10-perylenetetracarboxylic dianhydride (PTCDA) and graphene, Gan *et al.* found that the ECL intensity of peroxydisulfate solution can be amplified by graphene–PTCDA nanocomposites, and based on this, an ultrasensitive ECL sandwich-type aptasensor was developed for thrombin detection.[10] Furthermore, based on the nanocomposites of electrochemically reduced graphene oxide (ERGO) and Au NPs, which were electrochemically prepared by a two-step reduction method, the ECL intensity of peroxydisulfate was enhanced and further a label-free ECL immunosensor towards human IgG was proposed.[21] All the results above showed that graphene and graphene-based nanocomposites exhibited great potential in

[a]*Key Laboratory of Modern Agriculture Equipment and Technology, School of Chemistry and Chemical Engineering, Jiangsu University, Zhenjiang, 212013, P.R. China. E-mail: wangkun@ujs.edu.cn; Fax: +86 511 88791708; Tel: +86 511 88791800*
[b]*School of Food and Biological Engineering, Jiangsu University, Zhenjiang, 212013, P.R. China*

† Electronic supplementary information (ESI) available. See DOI: 10.1039/c3an01533e

the ECL system, and it is of great necessity to explore them in the field of biosensing applications.

Dopamine (DA) is an important neurotransmitter in the mammalian central nervous system and plays a very important role in the renal, hormonal, and cardiovascular systems.[22,23] Until now, several impressive techniques have demonstrated the feasibility for the assay of DA, including electrochemical,[24] spectrophotometry[25] and high performance liquid chromatography methods.[26] However, these approaches suffer from drawbacks including long-time consumption, high cost, and lack of high sensitivity.[27,28] Thus, considerable efforts have been devoted to overcoming these problems, in which the ECL technique is a most important and successful method for this purpose. In this paper, with the synergistic amplification of Au NPs and reduced graphene oxide (RGO), a novel strategy to amplify the ECL signal of peroxydisulfate solution was developed, and based on this, an ECL biosensor for sensitive and selective detection of dopamine (DA) was constructed. In particular, this approach would hold a new perspective to apply the ECL system of peroxydisulfate in bioassays.

Experimental

Reagents

Chloroauric acid ($HAuCl_4$), sodium oleate ($C_{18}H_{33}NaO_2$), hexamethylenetetramine (HMTA), dimethyl formamide (DMF) and $K_2S_2O_8$ were purchased from Sinopharm Chemical Reagent Co., Ltd. DA was obtained from Sigma-Aldrich. PBS (phosphate buffered solution, 0.1 M) of various pH values were prepared by mixing stock standard solutions of NaH_2PO_4 and Na_2HPO_4, and the pH was adjusted with 0.1 M NaOH solution. Other reagents were of analytical grade and used as received without further purification, and all solutions were prepared with twice-distilled water.

Apparatus

The transmission electron microscopy (TEM) image was taken with a JEOL 2100 transmission electron microscope (JEOL, Japan) operated at 200 kV. The Fourier transform infrared (FT-IR) and Raman spectra were obtained using a Nicolet Nexus 470 FT-IR spectrometer and a RM 2000 microscopic confocal Raman spectrometer, respectively.

Electrochemical impedance spectroscopy (EIS) was performed in a 0.1 M KCl solution containing 5 mM $Fe(CN)_6^{3-/4-}$ with a frequency range from 0.01 Hz to 10 kHz at 0.23 V, and the amplitude of the applied sine wave potential in each case was 5 mV which was taken with a ZENNIUM electrochemical workstation (Zahner Instruments, Germany). Electrochemical signals were recorded using a CHI660 B electrochemical analyzer (Chen Hua Instruments, Shanghai, China) and ECL curves were recorded using a Model MPI-A ECL analyzer system (Xi'an Remax Electronic Science and Technology Co. Ltd, Xi'an, China). The photomultiplier tube (PMT) was biased at 800 V in the process of detection. All electrochemical and ECL curves were recorded using a conventional three-electrode system where a glassy carbon electrode (GCE, 3 mm in diameter) was used as a working electrode, a Ag/AgCl (saturated KCl solution) as a reference electrode and platinum wire as a counter electrode, respectively. The electrochemical measurements were performed in the potential range of 0 to −1.6 V with a scan rate of 100 mV s^{-1}.

Preparation of Au NP–RGO

Au nanoparticle decorated reduced graphene oxide (Au NP–RGO) was synthesized according to the as-reported method.[29] Briefly, 0.625 mL of 2% $HAuCl_4$ was diluted in 0.625 mL of 0.2 M HCl solution, then 10 mL of 0.004 M $C_{18}H_{33}NaO_2$ solution was added under stirring until the color turned lemon. Next, 10 mg GO prepared by the modified Hummers' method[30] was added to the above solution, and 0.055 g HMTA was mixed under stirring for 10 min. Meanwhile, the pH of this mixture was adjusted to 13 with 0.4 M KOH. Subsequently, the mixture was kept at 80 °C in an oil bath under stirring for 80 min until the color of the solution changed to amaranth. Finally, the resulting suspension was centrifuged and washed three times with distilled water and ethanol, and dried in a vacuum at 50 °C for 24 h.

Fabrication of the modified electrodes

Prior to modification, the GCE was firstly polished with sand paper followed by 1.0, 0.3, and 0.05 μm alumina slurry, respectively, and then sonicated in water to remove any residues. The procedure for the preparation of the modified electrodes was described as follows: 1.0 mg Au NP–RGO was dispersed in 0.5 mL DMF to make a Au NP–RGO homogeneous suspension, then 6 μL of this suspension was cast onto the pretreated GCE surface and dried in air at room temperature to form the Au NP–RGO modified GCE (denoted as Au NP–RGO/GCE). The Au NP–RGO/GCE was rinsed with water several times prior to use. As a comparison, 6 μL of 2.0 mg mL^{-1} RGO and Au NP suspension were used to fabricate the RGO/GCE and Au NP/GCE, respectively.

Results and discussion

Characterization of the Au NP–RGO

Fig. 1A displays the FT-IR spectra of the as-prepared GO and Au NP–RGO. The GO exhibits the characteristic peaks observed at 1070 cm^{-1}, 1412 cm^{-1}, 1625 cm^{-1} and 1736 cm^{-1} (curve a), which are in agreement with a previous report.[31] In contrast, for Au NP–RGO (curve b), the peaks at 1412 cm^{-1} and 1736 cm^{-1} disappeared. Moreover, the C=C skeletal vibrations of unoxidized graphitic bands increased in intensity and shifted to lower wavenumbers, which indicated that the GO has been reduced to RGO in the reaction process.

Raman spectroscopy is considered to be an efficient tool for characterizing carbon materials, and the intensity ratio of D- and G-band (I_D/I_G) is a measure of disorder degree and average size of the sp^2 domains.[32] The Raman spectrum of GO (curve a, Fig. 1B) shows the characteristic GO peaks at around 1350 cm^{-1} (D-band) and 1584 cm^{-1} (G-band) with an intensity ratio I_D/I_G of 0.95. In the spectrum of Au NP–RGO (curve b, Fig. 1B), the value of I_D/I_G is increased from 0.95 to 1.02, and moreover the bands slightly blue-shift to around 1343 cm^{-1} and

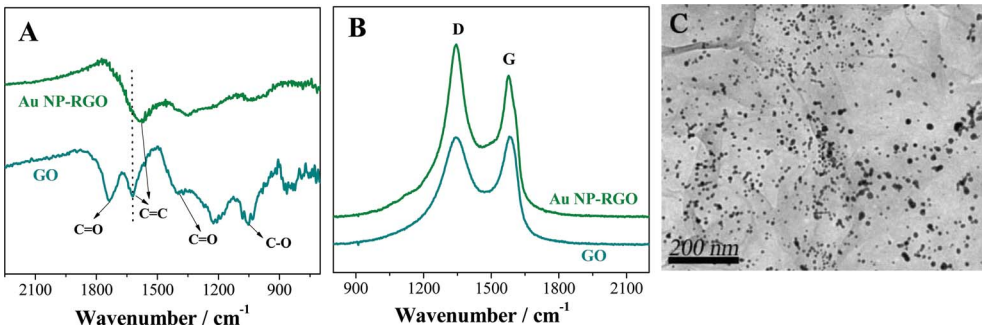

Fig. 1 (A) FT-IR and (B) Raman spectra of GO (a) and Au NP–RGO (b); (C) TEM image of Au NP–RGO.

1578 cm^{-1}, which further proved that the GO has been reduced during the chemical process.[31] Fig. 1C displays the TEM image of the resulting Au NP–RGO. It is obvious that the nanocomposites retained a two-dimensional sheet structure with micrometers-long wrinkles, and the Au NPs with an average size of 12 nm were decorated well on the surface of RGO.

Electrochemical and ECL behaviors of the Au NP–RGO modified electrode

Using $Fe(CN)_6^{3-/4-}$ as the electrochemical probe, the Nyquist plots of different electrodes were obtained (Fig. 2A). Obviously, the charge transfer resistance (R_{ct}) at the RGO/GCE (curve b) and Au NP/GCE (curve c) is smaller than that at the bare GCE (curve a), revealing that both RGO and Au NPs could act as a good electron-transfer interface between the electrochemical probe and the electrodes.[33] Moreover, when Au NP–RGO was incorporated into the electrochemical system, it was obvious that the R_{ct} is much smaller, indicating that the Au NP–RGO could facilitate the electron-transfer more effectively than Au NPs or RGO.[34]

Furthermore, the ECL behaviors of the bare GCE, RGO/GCE, Au NP/GCE and Au NP–RGO/GCE were compared in 0.1 M PBS containing 0.05 M $K_2S_2O_8$ (Fig. 2B). It is clear that the ECL signal of the Au NP–RGO/GCE (curve d) was much higher than that of the bare GCE (curve a), RGO/GCE (curve b) and Au NP/GCE (curve c), suggesting that the Au NP–RGO could enhance the ECL signal of $K_2S_2O_8$ effectively, which is due to the synergetic effect of RGO and Au NPs in the Au NP–RGO film. In addition, the ECL intensity of $K_2S_2O_8$ solution on the Au NP–RGO modified electrode is about 5-fold higher than at the nanocomposites of ERGO and Au NPs, which were prepared by a two-step electrochemical reduction method.[21] Thus, in order to achieve the optimal ECL response, the ECL behaviors of Au NP–RGO were investigated for the detection of analytes in our experiment.

Cyclic voltammograms (CVs) of the bare GCE and Au NP–RGO/GCE in 0.1 M PBS in the absence and presence of 0.05 M $K_2S_2O_8$ were studied, as shown in Fig. 3A and C. For the bare GCE in PBS (curve a, Fig. 3A), there was a reduction peak at −0.91 V that resulted from reduction of dissolved oxygen in solutions.[35] After adding 0.05 M $K_2S_2O_8$ (curve b, Fig. 3A), a cathodic peak was observed at −1.02 V, which was ascribed to the reduction peak of $K_2S_2O_8$ and the overlap peak of dissolved oxygen.[11,36] For the Au NP–RGO/GCE (Fig. 3C), the reduction peak of $K_2S_2O_8$ shifted positively to −0.72 V, and the peak current was about 2.1-fold higher than that of the bare GCE, which suggested that the Au NP–RGO could catalyze the reduction of $K_2S_2O_8$.[37,38]

Fig. 3B and D show the corresponding ECL behaviors of the bare GCE and Au NP–RGO/GCE in 0.1 M PBS in the absence and presence of 0.05 M $K_2S_2O_8$. It can be seen that no light emission was observed on either the bare GCE or the Au NP–RGO modified GCE in PBS. However, with 0.05 M $K_2S_2O_8$ added, ECL emission was observed at both the bare GCE and the Au

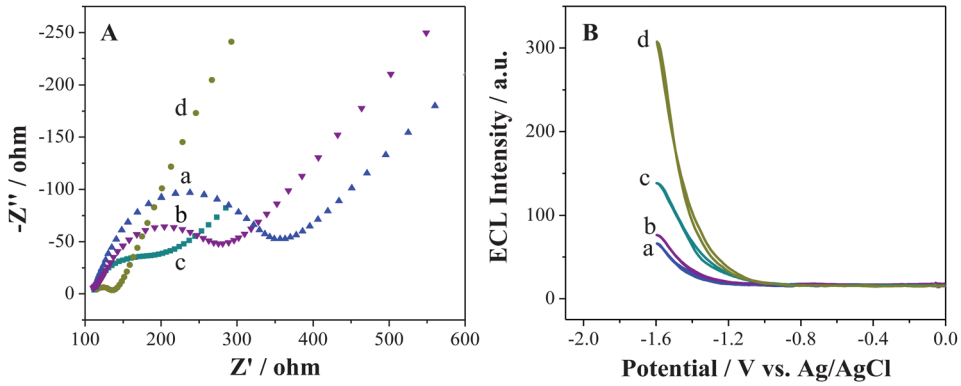

Fig. 2 (A) EIS of bare GCE (a), RGO/GCE (b), Au NP/GCE (c) and Au NP–RGO/GCE (d) in 0.1 M KCl containing 5 mM $Fe(CN)_6^{3-/4-}$; (B) ECL behaviors of bare GCE (a), RGO/GCE (b), Au NP/GCE (c) and Au NP–RGO/GCE (d) in 0.1 M PBS (pH 7.4) containing 0.05 M $K_2S_2O_8$.

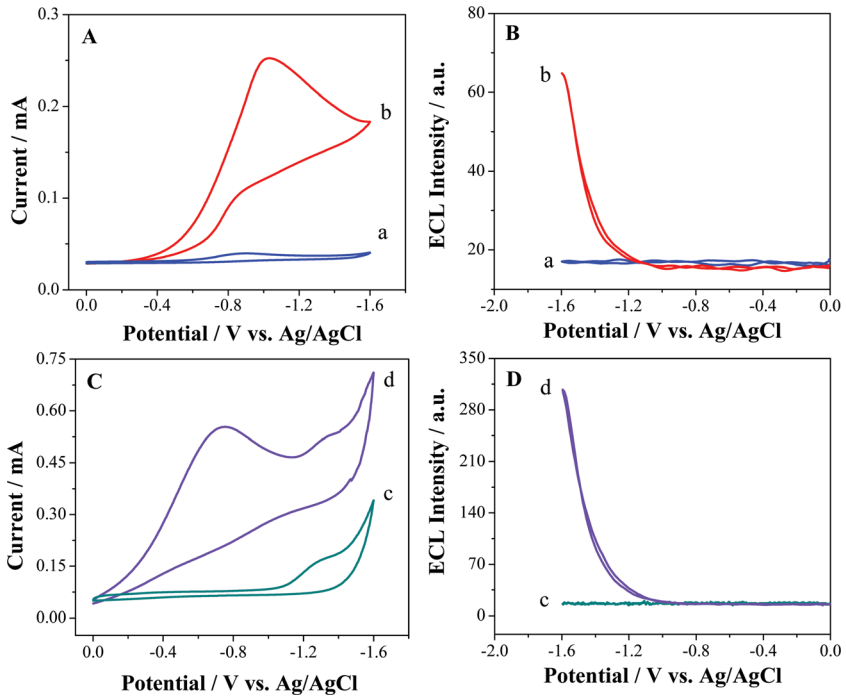

Fig. 3 (A) CVs and (B) ECL curves of the bare GCE in 0.1 M PBS (pH 7.4) in the absence (a) and presence (b) of 0.05 M $K_2S_2O_8$; (C) CVs and (D) ECL curves of the Au NP–RGO/GCE in 0.1 M PBS (pH 7.4) in the absence (c) and presence (d) of 0.05 M $K_2S_2O_8$.

NP–RGO/GCE, which indicated that the ECL emission was produced from the $S_2O_8^{2-}$. And the possible ECL mechanism is as follows:[11]

$$K_2S_2O_8 + e \rightarrow SO_4^{\cdot -} + SO_4^{2-} \quad (1)$$

$$SO_4^{\cdot -} + H_2O \rightarrow HO^{\cdot} + HSO_4^{-} \quad (2)$$

$$HO^{\cdot} \rightarrow HOO^{\cdot} + H_2O \quad (3)$$

$$O_2 + H_2O + e \rightarrow HOO^{\cdot} + HO^{-} \quad (4)$$

$$SO_4^{\cdot -} + HOO^{\cdot} \rightarrow HSO_4 + {}^1(O_2)_2^{*} \quad (5)$$

$${}^1(O_2)_2^{*} \rightarrow 2{}^3O_2 + h\nu \quad (6)$$

In addition, the ECL intensity of the Au NP–RGO/GCE was about 5-fold higher than that of the bare GCE with the ECL onset potential positively shifted from −1.2 V to −0.9 V, indicating that the Au NP–RGO can catalyze the reduction of $S_2O_8^{2-}$ to $SO_4^{\cdot -}$ effectively.[37,39]

Optimization of experimental conditions

In order to achieve the optimal ECL response, the effects of the $K_2S_2O_8$ concentration and solution pH on the ECL behavior of the Au NP–RGO modified electrode were considered carefully.

As shown in Fig. S1A and B,† the ECL intensity increased gradually with the increase of the $K_2S_2O_8$ concentration. However, when the $K_2S_2O_8$ concentration reached 0.05 M, the ECL intensity increased slowly and tended to a stable signal.

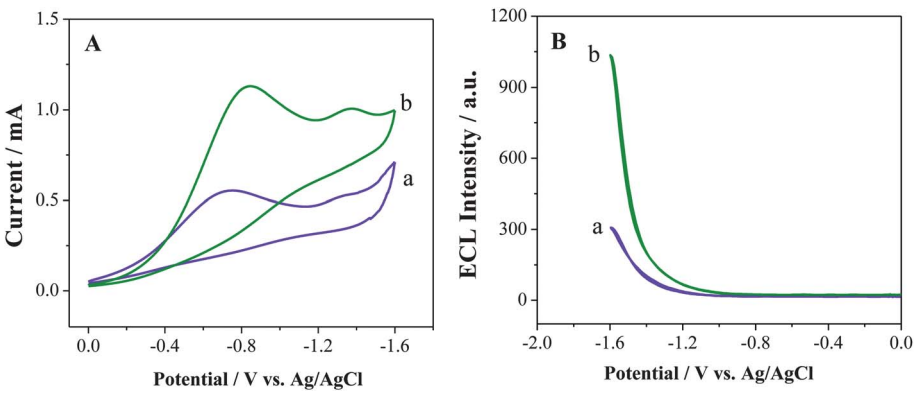

Fig. 4 (A) CVs and (B) ECL–potential curves of the Au NP–RGO/GCE in PBS (pH 7.4) containing 0.05 M $K_2S_2O_8$ without (a) and with (b) 10 μM DA.

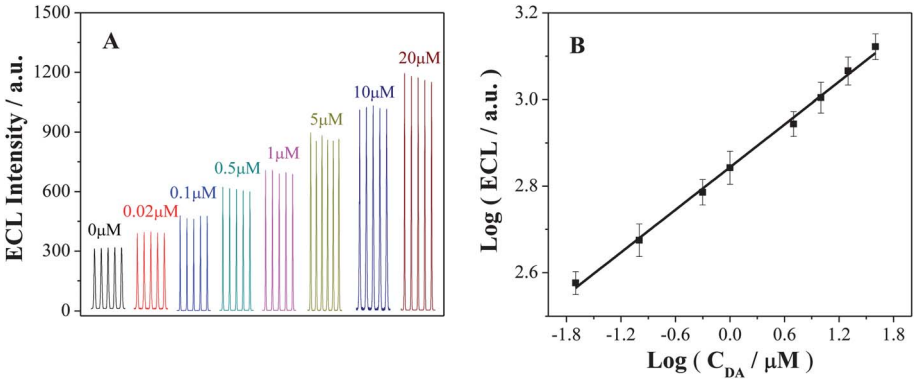

Fig. 5 (A) Effect of the DA concentration on ECL behaviors of the Au NP–RGO/GCE in 0.1 M PBS (pH 7.4) with 0.05 M $K_2S_2O_8$; (B) calibration curve for DA detection. Error bars: ±S.D., $n = 3$.

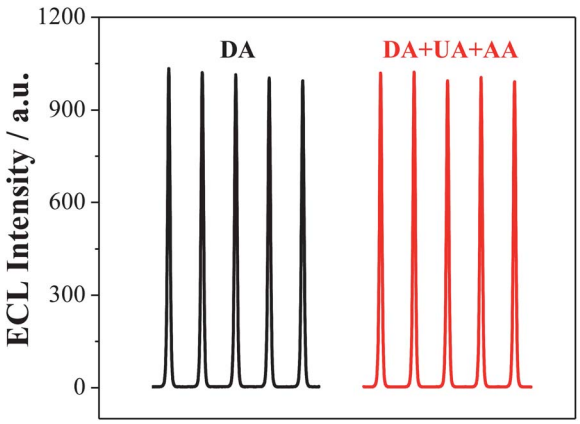

Fig. 6 Consecutive ECL intensity of the Au NP–RGO/GCE in the absence and presence of interfering agents.

Thus, 0.05 M was chosen as the optimal concentration of $K_2S_2O_8$ in this experiment.

The effect of pH on the ECL behavior of the Au NP–RGO modified electrode was performed in 0.1 M PBS containing 0.05 M $K_2S_2O_8$ with the pH range of 6.0–9.0. As shown in Fig. S1C and D,† the ECL intensity increased with the increase of pH from 6.0 to 7.4 and then dropped at high pH from 7.4 to 9.0. The possible mechanism is as follows: at low pH, the proton could be reduced easily at the negative potential and thus the electro-reduction of Au NP–RGO is inhibited and at pH 9.0, the strong oxidant $SO_4^{\cdot-}$ is consumed *via* the scavenging effect of OH^-.[37–41] Thus, pH 7.4 was chosen as the optimal pH value in this experiment.

ECL detection of DA based on the Au NP–RGO modified electrode

More interestingly, when DA was injected into the above electrolyte, it was obvious that the ECL intensity enhanced by about 3.6-fold (Fig. 4B), and additionally, the peak current was much higher (Fig. 4A), indicating that the DA could indeed facilitate the electrochemical behavior of $S_2O_8^{2-}$ in solution.

Based on the results above and under optimized conditions, we explored the quantitative range of the proposed ECL sensor for DA detection. Fig. 5A presents the effect of different concentrations of DA on the ECL intensity of the Au NP–RGO modified electrode. It is clear that the ECL intensity increases with the increase of DA concentration, and the standard calibration curve for DA detection is illustrated in Fig. 5B, which shows that the logarithm of ECL intensity increased linearly with the logarithm of DA concentration in the range from 0.02–40 μM with a correlation coefficient of 0.997. The detection limit was 6.7 nM ($S/N = 3$). In addition, compared with previous reports for ECL biosensors towards DA,[12,40–42] this work shows a wider linear response with lower detection limit (Table S1†).

Stability and interference

The stability of the Au NP–RGO modified electrode and the interferences of electroactive species with the DA response were examined at their physiological normal levels. Fig. 6 shows a stable ECL signal under consecutive potential scans from 0 to −1.6 V for 5 cycles with 10 μM DA in the electrolyte. An interference investigation was performed by using the solution containing 10 μM of DA and 20 μM of ascorbic acid and uric acid respectively, which are two common interfering agents for DA detection. Almost no obvious change could be observed, indicating an acceptable selectivity for DA detection.

Sample analysis

In order to investigate the possible application of the ECL biosensor in clinical analysis, the Au NP–RGO modified electrode has been employed for the detection of the DA concentration in human plasma utilizing a standard addition method without sample pretreatment. The concentration of DA was determined to be 1.7 μM, and the recovery tests were performed by adding 5 μM DA to the sample. The corresponding results are listed in Table S2,† and the average recoveries ranged between 97.0% and 101.5%, ascertaining the practical application of the proposed DA biosensor in clinical analysis.

Conclusions

In this paper, based on the synergistic amplification of Au NPs and RGO, a novel strategy to amplify the ECL signal of

peroxydisulfate solution was constructed and an ECL biosensor for DA detection was developed. Compared with the bare electrode, the Au NP–RGO modified electrode could not only enhance the ECL intensity of peroxydisulfate solution, but also decrease the onset potential. In addition, the ECL intensity could be amplified effectively by DA, based on which an ECL biosensor for DA was constructed. In addition, the ECL biosensor showed acceptable accuracy and precision for the detection of DA. Therefore, this work provided a new method for signal amplification of peroxydisulfate ECL and would extend the application of peroxydisulfate in bioanalysis.

Acknowledgements

The present work was supported by the National Natural Science Foundation of China (no. 21175061, 21375050, 21305052 and 31271620), Program of Natural Science Foundation of Education Bureau of Jiangsu Province, China (no. 10KJA470007 and 13KJB210004), Key Laboratory of Modern Agriculture Equipment and Technology (no. NZ201109), China Postdoctoral Science Foundation (no. 2012M520998 and 2012M511217), and Innovation Project of Science and Technology for College Graduates of Jiangsu Province (no. CXZZ12_0704).

References

1 P. Bertoncello and R. J. Forster, *Biosens. Bioelectron.*, 2009, **24**, 3191–3200.
2 M. M. Richer, *Chem. Rev.*, 2004, **104**, 3003–3036.
3 M. H. Chiu, W. C. Wei and J. M. Zen, *Electrochem. Commun.*, 2011, **13**, 605–607.
4 L. L. Xue, L. H. Guo, B. Qiu, Z. Y. Lin and G. N. Chen, *Electrochem. Commun.*, 2009, **11**, 1579–1582.
5 R. Lei, X. Xu, F. Yu, N. Li, H. W. Liu and K. Li, *Talanta*, 2008, **75**, 1068–1074.
6 Y. Wang, J. Lu, L. H. Tang, H. X. Chang and J. H. Li, *Anal. Chem.*, 2009, **81**, 9710–9715.
7 L. Dennany, M. Gerlach, S. O'Carroll, T. E. Keyes, R. J. Forster and P. Bertoncello, *J. Mater. Chem.*, 2011, **21**, 13984–13990.
8 H. J. Wang, R. Yuan, Y. Q. Chai, H. Niu, Y. L. Cao and H. J. Liu, *Biosens. Bioelectron.*, 2012, **37**, 6–10.
9 G. F. Jie, H. P. Huang, X. L. Sun and J. J. Zhu, *Biosens. Bioelectron.*, 2008, **23**, 1896–1899.
10 X. X. Gan, R. Yuan, Y. Q. Chai, Y. L. Yuan, Y. L. Cao, Y. H. Liao and H. J. Liu, *Anal. Chim. Acta*, 2012, **726**, 67–72.
11 H. Niu, R. Yuan, Y. Q. Chai, L. Mao, Y. L. Yuan, Y. Zhuo, S. R. Yuan and X. Yang, *Biosens. Bioelectron.*, 2011, **26**, 3175–3180.
12 L. L. Li, H. Y. Liu, Y. Y. Shen, J. R. Zhang and J. J. Zhu, *Anal. Chem.*, 2011, **83**, 661–685.
13 H. Niu, R. Yuan, Y. Q. Chai, L. Mao, H. J. Liu and Y. L. Cao, *Biosens. Bioelectron.*, 2013, **39**, 296–299.
14 H. Niu, R. Yuan, Y. Q. Chai, L. Mao, Y. L. Yuan, Y. L. Cao and Y. Zhuo, *Chem. Commun.*, 2011, **47**, 8397–8399.
15 L. Qian and X. R. Yang, *Electrochem. Commun.*, 2007, **9**, 393–397.
16 T. Kuila, S. Boseet, A. K. Mishra, P. Khanra, N. H. Kim and J. H. Lee, *Prog. Mater. Sci.*, 2012, **57**, 1061–1105.
17 B. L. Su, D. P. Tang, Q. F. Li, J. Tang and G. N. Chen, *Anal. Chim. Acta*, 2011, **692**, 116–124.
18 W. H. Gao, Y. S. Chen, J. Xi, A. Zhang, Y. W. Chen, F. S. Lu and Z. G. Chen, *Sens. Actuators, B*, 2012, **171**, 1159–1165.
19 Y. J. Guo, S. J. Guo, J. Li, E. K. Wang and S. J. Dong, *Talanta*, 2011, **84**, 60–64.
20 K. Wang, Q. Liu, X. Y. Wu, Q. M. Guan and H. N. Li, *Talanta*, 2010, **82**, 372–376.
21 S. S. Peng, G. Z. Zou and X. L. Zhang, *J. Electroanal. Chem.*, 2012, **686**, 25–31.
22 J. W. Mo and B. Ogorevc, *Anal. Chem.*, 2001, **73**, 1196–1202.
23 R. M. Wightman, L. J. May and A. C. Michael, *Anal. Chem.*, 1988, **60**, 769A–779A.
24 A. Salmanipour and M. A. Taher, *Analyst*, 2011, **136**, 545–549.
25 M. R. Moghadam, S. Dadfarnia, A. M. H. Shabani and P. Shahbazikhah, *Anal. Biochem.*, 2011, **410**, 289–295.
26 V. Carrera, E. Sabater, E. Vilanova and M. A. Sogorb, *J. Chromatogr., B*, 2007, **847**, 88–94.
27 C. L. Sun, C. T. Chang, H. H. Lee, J. Zhou, J. Wang, T. K. Sham and W. F. Pong, *ACS Nano*, 2011, **5**, 7788–7795.
28 P. Bertoncello, P. J. Edgeworth, J. V. Macpherson and P. R. Unwin, *J. Am. Chem. Soc.*, 2007, **129**, 10982–10983.
29 J. G. Hu, F. H. Li, K. K. Wang, D. X. Han, Q. X. Zhang, J. H. Yuan and L. Niu, *Talanta*, 2012, **93**, 345–349.
30 W. S. Hummers and R. E. Offeman, *J. Am. Chem. Soc.*, 1958, **80**, 1339.
31 T. S. Sreeprasad, A. K. Samal and T. Pradeep, *J. Phys. Chem. C*, 2009, **113**, 1727–1737.
32 C. Gomez-Navarro, R. T. Weitz, A. M. Bittner, M. Scolari, A. Mews, M. Burghard and K. Kern, *Nano Lett.*, 2007, **7**, 3499–3503.
33 Y. Z. Zhang and W. Jiang, *Electrochim. Acta*, 2012, **71**, 239–245.
34 S. Liu, J. Yan, G. W. He, D. D. Zhong, J. X. Chen, L. Y. Shi, X. M. Zhou and H. J. Jiang, *J. Electroanal. Chem.*, 2012, **672**, 40–44.
35 Z. Y. Lin, Y. Liu and G. N. Chen, *Electrochem. Commun.*, 2008, **10**, 1629–1632.
36 G. F. Jie, B. Liu, H. C. Pan, J. J. Zhu and H. Y. Chen, *Anal. Chem.*, 2007, **79**, 5574–5581.
37 Y. Wu, L. Wang, H. Y. Wang and X. L. Zhang, *Electrochim. Acta*, 2008, **54**, 733–737.
38 Z. F. Chen, K. M. C. Wong, E. C. H. Kwok, N. Y. Zhu, Y. B. Zu and V. W. W. Yam, *Inorg. Chem.*, 2011, **50**, 2125–2132.
39 C. M. Cheng, Y. Huang, X. Q. Tian, B. Z. Zheng, Y. Li, H. Y. Yuan, D. Xiao, S. P. Xie and M. M. F. Choi, *Anal. Chem.*, 2012, **84**, 4754–4759.
40 X. Liu, L. X. Cheng, J. P. Lei and H. X. Ju, *Analyst*, 2008, **133**, 1161–1163.
41 R. Cui, Y. P. Gu, L. Bao, J. Y. Zhao, B. P. Qi, Z. L. Zhang, Z. X. Xie and D. W. Pang, *Anal. Chem.*, 2012, **84**, 8932–8935.
42 F. R. Sun, F. F. Chen, W. J. Fei, L. Sun and Y. Wu, *Sens. Actuators, B*, 2012, **706**, 166–167.

